# Effect of thermal residual stresses on ductile-to-brittle transition of a bi-material specimen by using the CAFE method

Yang Li [a], Xiaobo Ren [b], Jianying He [a], Zhiliang Zhang [a,*]

[a] NTNU Nanomechanical Lab, Department of Structural Engineering, Norwegian University of Science and Technology (NTNU), Richard Birkelands vei 1A, N-7491 Trondheim, Norway
[b] SINTEF Industry, Richard Birkelands vei 2B, N-7465 Trondheim, Norway

## ARTICLE INFO

## ABSTRACT

The effect of residual stress on fracture of materials or structures has been widely studied. However, its influence on ductile-to-brittle transition (DBT), a crucial phenomenon of structural materials, has rarely been investigated so far. In the present study, employing the eigenstrain method residual stresses are introduced into a bi-material specimen, where two configurations of crack and interface, e.g., one with interface perpendicular and one parallel to the crack extension, are designed to study the influence of residual stress. The DBT of the bi-material specimen in the presence of residual stresses is numerically studied by using the CAFE method where temperature dependent surface energy is implemented to calculate absorbed energy of Charpy impact testing specimen. It is found that residual stress generated in the two configurations affect the DBT in a similar manner. The DBT curves generally shift to higher temperature due to the decrease of absorbed energy with the increase of residual stress. It is found that the decrease of absorbed energy in both configurations is caused by the additional constraint on the notch root, which is induced by the residual stress and can facilitate the fracture.

## 1. Introduction

Residual stresses are those stresses maintained within a body without external load, which are stationary and at equilibrium with their surroundings (Withers, 2007). Residual stresses are caused by incompatible internal permanent strains induced by inelastic deformation, temperature gradients, or phase transformations during manufacturing and processing of the components. Residual stresses have a non-negligible influence on the safety of engineering structures, for instance, for plastic collapse, fracture, fatigue, creep, stress corrosion, and structural integrity. Several aspects regarding the influence of residual stresses on fracture have been investigated, e.g., crack driving force (Lei et al., 2000; Meith and Hill, 2002), crack tip constraint (Liu et al., 2008; Panontin and Hill, 1996; Ren et al., 2009), ductile fracture (Coules et al., 2018; Mahmoudi et al., 2008; Mirzaee-Sisan et al., 2008; Nose et al., 2017; Ren et al., 2010), brittle fracture (Hill and Panontin, 1999; Mirzaee-Sisan et al., 2007; Moshayedi and Sattari-Far, 2015; Ren et al., 2011), hydrogen embrittlement (Niwa et al., 2015; Toribio et al., 2011). The effect of residual stresses on transition of fracture from ductile to brittle (DBT) which is a crucial phenomenon of structural materials, e.g., steel, however, has received less attention so far.

Residual stresses occur inherently in materials or structures, for example welded joints, composite, layered structure etc., with a mismatch of coefficient of thermal expansion (CTE), when cooled down from an elevated temperature. Like the mismatch of material properties, e.g., elastic modulus, yield stress and strain hardening, the variation of CTE is also an origin of the heterogeneity of graded materials. In a 2D body containing a crack and sharp interface (perpendicular to the crack propagation), when the material properties exhibit a jump at the interface, the configuration forces at the interface could induce a contribution to the crack driving force (Kolednik et al., 2010). This contribution, namely additional driving force, induced by the material heterogeneity, can be described with a material inhomogeneity term (Simha et al., 2003, 2005), $C_{inh}$. Then, the effective crack-driving force at crack tip, represented by the local J-integral, $J_{tip}$, is defined by the sum of the far-field applied J-integral, $J_{app}$, and the material inhomogeneity term (Simha et al., 2003, 2005):

$$J_{tip} = J_{app} + C_{inh} \tag{1}$$

In this regard, a shielding/anti-shielding effect can be brought onto the crack tip, which depends on the magnitude of $C_{inh}$, in a negative or

---

positive manner. The effect of material inhomogeneity has been explored for linear-elastic and elastic-plastic bi-material systems with sharp and graded interfaces (Simha et al., 2003, 2005, 2008). The mismatch in elastic modulus, yield stress and strain hardening exponent at the interface has been investigated (Kolednik et al., 2005; Simha et al., 2003, 2005, 2008). The pronounced anti-shielding effect or shielding effect resulted by residual stresses in the bi-material system with mismatch of CTE has also been investigated (Chen et al., 2007; Fischer et al., 2007; Rakin et al., 2009). However, these studies of the effect of additional driving force on crack tip due to the thermal mismatch only have been performed under two dimensional and quasi-static conditions, and crack propagation has not been involved. In the present work, inspired by the studies on the effect of material inhomogeneity on fracture, two configurations of crack pertaining to the interface within a bi-material specimen with mismatch of CTE are designed to study the influence of residual stresses on DBT.

Although DBT has been well-studied in the past years, there is still a challenge to numerically describe the competition of two failure mechanisms of fracture in the transition region, e.g., ductile damage versus cleavage. A method, coupled finite element (FE) and cellular automat (CA), namely CAFE method proposed by Shterenlikht et al. (Shterenlikht, 2003; Shterenlikht and Howard, 2004, 2006) not only solves this problem but also represents the essential statistical features of microstructures of materials. In addition, a physically-based variable, the effective surface energy for cleavage propagation, has been established in our previous work (Li et al., 2019) to characterize the temperature dependent fracture toughness in the transition region. The CAFE method implemented with such an effective surface energy is applied to simulate the DBT of the bi-material specimen in present work. Then, the effect of residual stresses in two designed configurations on DBT is studied. In the end, the essential failure mechanisms induced by the residual stresses are discussed.

## 2. The CAFE method

To solve the difficulties associated with combined structural and microstructural interactions by using finite element methods, the structure and material is separated into two independent entities following the CAFE method (Shterenlikht, 2003). In this method, a set of CA arrays captures the mechanical essentials of the microstructural features, while finite elements process and hold the stress and strains at the structural level, which allows the evolving microstructural change to be analyzed. The implementation of above strategy to investigate the fracture behavior of Charpy specimen where ductile and brittle micromechanics work simultaneously, is presented in Fig. 1. The explicit
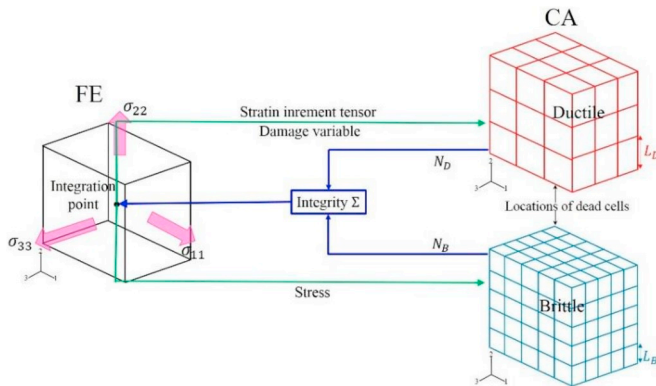
dynamic process has been employed to implement CAFE in finite element method so that crack propagation along a natural failure path can be numerically achieved through element removal. The strain increment tensor and damage variable in a single Gauss point of a finite element are distributed to the CA arrays. In each Gauss point, the relevant microstructural features are represented by two different arrays of cells, e.g., namely the ductile CA array and brittle CA array, which occupy the same amount of physical space. With the strain increment tensor and stress state at the structural level, ductile damage or cleavage fracture can be handled in ductile CA array or brittle CA array respectively according to the rule within the CA. The evolution of cells representing the development of microstructure of material, e.g., failure of the material in cells, is gathered by an integration indicator $\Sigma$ to communicate with the finite element calculations so that the failure of the element can be judged at the structural level. A VUMAT has been developed to apply the CAFE method in finite element analysis (Shterenlikht, 2003; Shterenlikht and Howard, 2004, 2006).

The CA arrays, non-deformable discrete-space and discrete-time entities, are mathematically assembled to the Gauss points. In the finite element solution, the strain increment at the associated Gauss point is uniformly distributed to the cells in the initial stage. The primary exchange occurs between the Gauss point and the ductile cells through the Rousselier model (Rousselier, 1987), which is employed to describe the constitutive behavior of ductile materials. Its plastic potential can be written as,

$$\frac{\sigma_{eq}}{\rho} + B(\beta)Dexp\left(\frac{\sigma_m}{\rho\sigma_1}\right) - H(\varepsilon_{eq}) = 0 \tag{2}$$

where $\sigma_{eq}$, $\sigma_m$ and $\varepsilon_{eq}$ are equivalent stress, mean stress and equivalent strain; $\sigma_1$ and $D$ are material constants that need to be tuned; $H(\varepsilon_{eq})$ is the hardening property of the material; $\rho$ is relative density, which can be described by

$$\rho = \frac{1}{1 - f_0 + f_0 exp\,\beta} \tag{3}$$

where $f_0$ is initial void volume fraction. $B(\beta)$ is the function of damage variable $\beta$, and $\beta$ is related to plastic deformation and damage which can be written as

$$\dot{\beta} = \dot{\lambda}Dexp\left(\frac{\sigma_m}{\rho\sigma_1}\right) \tag{4}$$

where $\dot{\lambda}$ is the plastic multiplier in the normality rule, $\lambda$ is proportional to the rate of equivalent plastic strain.

In the ductile CA arrays, since the large inclusions or carbides where void nucleated are uniformly distributed in the material, an experimentally measured distribution of the initial void volume fraction $f_0$ is spread over the ductile cells. $L_D$ is used to characterize the unit size of ductile damage of material, which normally relates to the spacing of large inclusions or carbides in steel. However, in practice the distribution of $f_0$ is substituted by a normal distribution of damage value $\beta_F$ in ductile CA array in order to circumvent the difficulty of convergence. It is assumed that the ductile damage occurs when damage variable reaches to its critical value $\beta_F$.

The local critical fracture stress for cleavage can be calculated as,

$$\sigma_F = \sqrt{\frac{\pi E \gamma_{eff}}{(1 - \nu^2)d_g}} \tag{5}$$

where $\gamma_{eff}$ is effective surface energy; $E$ and $\nu$ are Young's modulus and Poisson's ratio respectively; $d_g$ is grain size. In the CAFE method, $\eta$, the fraction of brittle cells, is adopted to represent grains with nucleated micro-crack within the particle in each brittle CA array. In the brittle CA arrays, the cleavage facet size $d_{CFS}$ is applied as the size of cells in brittle CA arrays, $L_B$, which can be measured through fractographic analysis on



**Fig. 1.** The illustration of the CAFE model in which ductile damage and cleavage fracture have been coupled through two different CA arrays. Here, where $N_D$ and $N_B$ are the number of 'dead' cells of ductile CA arrays and brittle CA arrays respectively to indicate the failure of material in the cells; $L_D$ and $L_B$ are the size of cells in brittle and ductile CA arrays.

the fracture surface of specimen (Shterenlikht and Howard, 2006). A distribution of grain size is also incorporated in the brittle cells to represent the intrinsic inhomogeneity of material. Since the high-angle grain boundary is naturally the barrier of cleavage crack propagation (Stec and Faleskog, 2009), a random orientation is assigned to each cell in brittle CA arrays, and a threshold of misorientation, $\theta_{th}$, is assumed so that crack can propagate from one cell to the other. The brittle fracture occurs when both the local stress exceed $\sigma_F$ and the orientation of the cell is smaller than the $\theta_{th}$.

The state of each cell in the next time increment is determined by the state of itself and its neighborhood at the current time increment. If the cell is failed due to the fracture propagation, the initial state of cell, e.g., 'alive', will be changed to 'dead'. Then, the strain/stress concentration will occur on the closing neighborhood of 'dead' cell since it loses the load-bearing capacity. A framework (Shterenlikht, 2003; Shterenlikht and Margetts, 2015) has been established to locate such a closing neighborhood around the 'dead' cell. The local concentration factors, $C_D$ for ductile CA array and $C_B$ for brittle CA array, are used to describe the strain/stress concentration occurring on the closing neighborhood when one cell is failed. Thus, at the next time increment, the states of concentrated cells (either ductile or brittle) are determined by the results of comparison between the product of damage variable and concentration factors with failure criteria mentioned above. An integrity indicator, $\Sigma$, is used to count the 'dead' cells of both ductile and brittle CA arrays by which the potential fracture at each time increment is evaluated. When $N_D$ or $N_B$ reaches its maximum value $N_{D-max}$ or $N_{B-max}$, the integrity indicator $\Sigma$ turns to be zero, which means material inside the integration point is failed and the integration point does not have load-bearing capacity any more. Then, the FE will be removed from the further calculations. The calculation of the integrity indicator can be described by

$$\Sigma = 1 - \max\left(\frac{N_D}{N_{D-max}}, \frac{N_B}{N_{B-max}}\right) \qquad (6)$$

It is assumed that if a cell in either array is dead, the cell in the other array will artificially become dead as well. This implies that the material in two arrays can only fail in either a brittle or a ductile manner. Since two failure modes are totally independent, the occurrence of fracture is a consequence of the competition between these two different failure mechanisms. More details about the CAFE method can be found in (Shterenlikht, 2003; Shterenlikht and Howard, 2006), and a flow chart of the calculation procedure of CAFE method has been presented in (Li et al., 2019).

To reveal the essence of temperature dependent fracture toughness in the transition region of BCC metals, a physically-based variable $\gamma_{eff}$, e. g., the effective surface energy of cleavage has been found (Li et al., 2018, 2019). Further, the effective surface energy for cleavage propagating across the grain boundary, e.g., $\gamma_{mm}$ is calculated by using a continuum approach proposed in our previous work (Li et al., 2019). By implementing this temperature dependent $\gamma_{mm}$ into the CAFE method, the DBT of TMCR steel has been successfully predicted comparing to the experimental results (Li et al., 2019). In this work, the CAFE method implemented with this validated $\gamma_{mm}$ will be adopted to study the influence of residual stresses on the DBT of a bi-material specimen of steel.

## 3. Numerical simulation

### 3.1. Residual stresses generation

In principle, the interface formed by the inhomogeneity of material, is inclined to the crack extension with any angle (Simha et al., 2003, 2005, 2008). In the present work, two extreme configurations, e.g., the interface perpendicular to crack extension (the mostly studied scenario in the literature (Chen et al., 2007; Fischer et al., 2007; Rakin et al., 2009)), and the interface in parallel to the crack propagation, are

designed in the bi-material specimen, see Fig. 2. In both configurations, the interface due to the inhomogeneity of material in the bi-material specimen is formed by a mismatch of CTE, namely $\Delta CTE$ denoted by $(\alpha_1 - \alpha_2)$, where $\alpha_1$ and $\alpha_2$ are the coefficient of thermal expansion. It is assumed that the thermal expansion in different region is isotropic. In practice, the configuration 1 can be found in a full-thickness testing specimen with a pre-crack, cutting from a repair weld (Aloraier et al., 2010) or a clad pipe fabricated via explosive welding process (Zamani and Liaghat, 2012), where the crack vertically propagates across the interface. The configuration 2 corresponds to a full-thickness testing specimen with a pre-crack extracted from a girth weld or butt weld in a pipeline (Faes et al., 2009), in which the pre-crack introduced in the weld meal extends in parallel to the interface formed by the weld and base metal. The difference is that a sharp crack in a CT type specimen (Chen et al., 2007; Fischer et al., 2007; Rakin et al., 2009) is substituted with a blunt notch in a Charpy specimen in the present work. Additionally, the other inhomogeneities of material, e.g., the mismatch of strength, strain hardening etc., are not considered here. Residual stresses in both configurations are generated by using eigenstrain method (Jun and Korsunsky, 2010; Mura, 1987) in a rapid cooling process. The thermal strain, namely, eigenstrain, induced by temperature change are given by

$$\varepsilon_{ij}^* = \alpha \Delta T \delta_{ij} \qquad (7)$$

where $\alpha$ is the coefficient of thermal expansion, $\Delta T$ is the temperature change and $\delta_{ij}$ is the unit tensor. Residual stresses are introduced by applying a unit temperature decrease into the regions with different CTE within the specimen.

### 3.2. Charpy impact test

Standard Charpy V-notch test is modelled by using an explicit dynamic process of Abaqus 6.14 and together with a subroutine of CAFE method introduced in section 2. According to the standard ASTM E23-18 (2018), the dimensions of the specimen are 55 mm (length), 10 mm (width) and 10 mm (depth), and the notch radius and depth are 0.25 mm and 2.0 mm respectively. The Charpy specimen is meshed with 8 nodes and reduced integration elements (C3D8R), see Fig. 3. A small region in the center of model with a finer mesh size, e.g., 0.5 mm, is the damage zone, where damage normally occurs and cell arrays are assembled. The other part of the Charpy specimen is modelled with an elastic-plastic material. The damage zone has 3560 elements, in total there are 20,
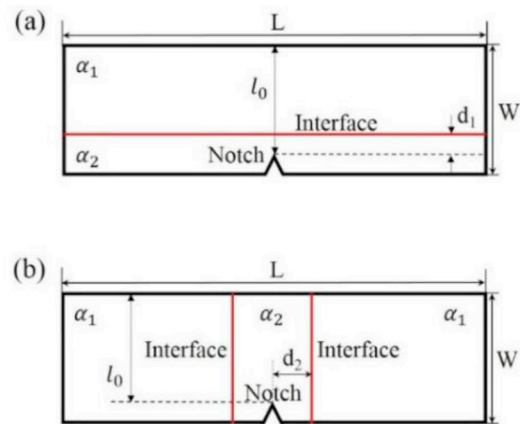


**Fig. 2.** 2D Configurations of the bi-material specimen with pre-notch and interface formed by the mismatch of CTE in the Charpy specimen: (a) interface perpendicular to the crack propagation; (b) interface parallel to the crack extension. Here, $d_1$ and $d_2$ are the distance of interface from the notch root; $l_0$ is the ligament of Charpy specimen; L is the length of specimen; W is the width of specimen.
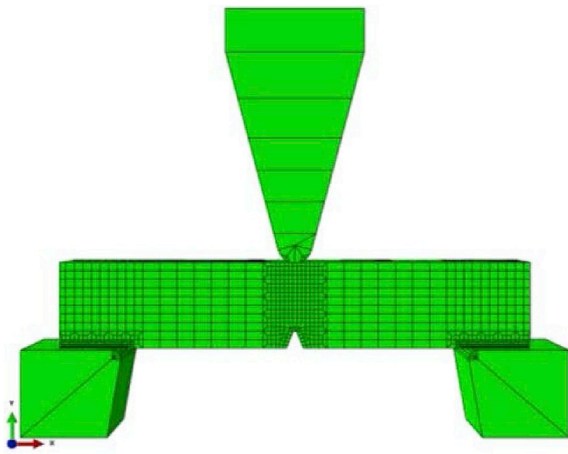
**Fig. 3.** Finite element model of Charpy V-notch impact test.

300 elements for the whole specimen. The striker and anvils are meshed with C3D8R/C3D6 type of elements, where the material is pure elastic. A friction coefficient 0.15 is adopted to simulate the contact between specimen and striker/anvils. The initial velocity of striker is 5.5 m/s.

The cell size of ductile CA arrays $L_D$ is assumed to be 125 $\mu m$. In addition, the cell size of brittle CA arrays $L_B$ is assumed to be 62.5 $\mu m$. Then, the number of cell in linear dimension, e.g., $m_D = 4$ in each ductile CA array. Similarly, there are 8 cells in linear dimension of each brittle CA array, e.g., $m_B = 8$. Accordingly, each element has 64 ductile cells and 512 brittle cells. There are in total 227840 ductile cells and 1822720 brittle cells in the damage zone. Once that the cells in one orthogonal section of either ductile or brittle CA array are failed, it is considered that the CA array has lost its load-bearing capacity. $N_{D-max}$ or $N_{B-max}$ in each CA array is 16 for ductile CA or 64 for the brittle CA array. The $C_D$

for ductile CA array is 1.4 and $C_B$ for brittle CA is 11.0 (Shterenlikht and Howard, 2006).

### 3.3. The material properties

As mentioned in section 3.1, the other inhomogenities of material in the bi-material specimen are not considered. It is assumed that the material properties in different regions are identical except for their CTE. Since the DBT of the TMCR steel has been successfully modelled and compared with available experimental results in our previous work (Li et al., 2019), in the present study the parameters related to the microstructure and material properties of the TMCR steel adopted in our previous work are applied to study the DBT of the bi-material specimen with the presence of residual stress (see section 3.1). The yield stress of the TMCR steel at room temperature is 447 MPa. The initial void volume fraction of the material $f_0$ is 0.0001. A normal distribution of the critical damage variable $\beta_F$ is used, in which $\beta_{F-mean}$ equals to 9.0 and the standard deviation $\beta_{F-std}$ equals to 1.2. The material constants $D$ and $\sigma_1$ in Rousellier model are 1.6 and 400 MPa respectively. The flow stress at different temperature and the grain size distribution of the TMCR steel are presented in Fig. 4 of the ref. (Li et al., 2019). A three-parameter Weibull distribution is used to describe the statistic feature of grain size distribution, in which the scale, shape and location parameter are 1.223, 5.392 and 0.516 respectively. The fraction of brittle CA cells where cleavage is nucleated, $\eta$, is assumed to be 0.01. The misorientation threshold $\theta_{th}$ is assumed to be 40°.

## 4. Results

### 4.1. Configuration 1

According to the description in section 3.1, the variable $\Delta CTE$ is adopted to generate different residual stresses in specimen through
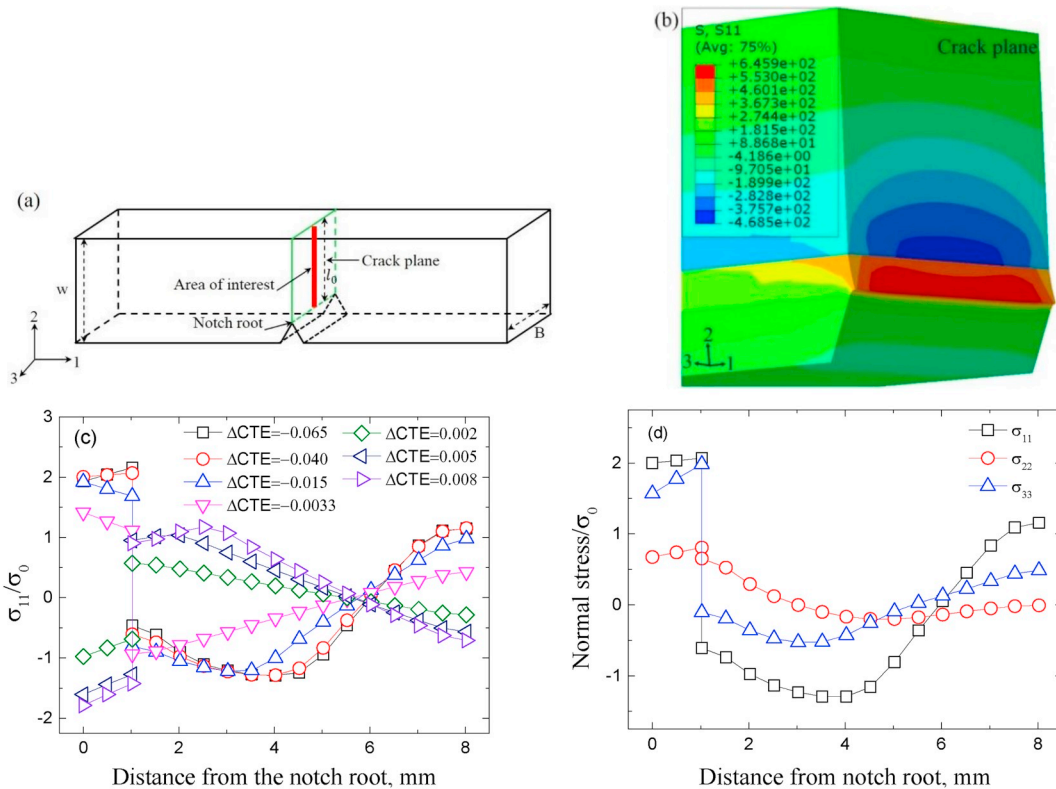


**Fig. 4.** Distribution of residual stresses at the center of Charpy specimen along the ligament when $d_1/l_0 = 0.125$ : (a) schematic of the region of interest, here B is the thickness of specimen, (b) the pattern of opening stress of the case with a $\Delta CTE$ = -0.0033°$C^{-1}$, (c) opening stress $\sigma_{11}$, (d) normal stresses with a $\Delta CTE$ = -0.04°$C^{-1}$.

changing $\alpha_2$ and fixing $\alpha_1$, in which $\alpha_1$ is assumed to be equal to $0.01°C^{-1}$. Meanwhile, the distance of interface away from the notch root normalized by the length of ligament, $d_1/l_0$, is used to depict the position of interface to the notch root. Firstly, $d_1/l_0 = 0.125$ is chosen for residual stresses generation. Since crack tip constraint in the middle of thickness is always the highest, the opening stress in the center of crack plane is more relevant, see Fig. 4(a). The detailed opening stress distribution for the case with a $\Delta CTE = $ -0.0033$°C^{-1}$, is presented in Fig. 4(b). An interface induced by the mismatch of CTE is clearly presented in the vicinity of notch root. Since more pronounced contraction occurs beneath the interface, an upward out-of-plane bending is generally produced in the specimen, and accordingly tensile stresses in the area between notch root and interface are generated, and the stresses above the interface turn to be compressive to keep balance. This indicated that an anti-shielding effect of interface and detrimental driving force on the crack front are induced by a negative $\Delta CTE$. The results agree with the findings by Rakin et al. (2009). The opening stresses $\sigma_{11}$ along the ligament in the middle of thickness normalized by the yield stress at room temperature, $\sigma_0$, for cases with variable $\Delta CTE$ are presented in Fig. 4(c). To better understand the distribution of residual stress, its normal components for the case with $\Delta CTE = $ -0.04$°C^{-1}$, at the center along the ligament vs. the distance from the notch root are potted in Fig. 4(d). It can be found that the other normal stresses distribute with a similar feature to that of opening stress, $\sigma_{11}$, and that the opening stress is higher than other normal stresses.

### 4.1.1. The influence of $d_1/l_0$ on impact toughness

The change of the distance between the interface and the notch root can also generate different residual stress field. For a constant $\Delta CTE = -0.04°C^{-1}$, the opening stresses along ligament in the center of specimen vs. the distance away from notch root are plotted in Fig. 5(a) with different $d_1/l_0$. It is observed that the opening stress decreases with the increase of $d_1/l_0$ and the distribution pattern of the opening stress is similar to that of the case with negative $\Delta CTE$ shown in Fig. 4(c). However, a compressive stress is found near the notch root for the case with $d_1/l_0 = 0.375$. This is because the bending is much further away from the notch root so that compressive deformation is generated near the notch root. The Charpy impact tests are modelled at different temperatures with residual stresses presented in Fig. 5(a). The absorbed energies of Charpy specimen vs. $d_1/l_0$ are plotted in Fig. 5(b), in which three runs are performed to reproduce the scattering feature according to the ASTM E23-18 (2018). The scattering results of absorbed energy produced by the CAFE method is induced by the input of the statistical information of the material, e.g., $\beta_F$, $d_g$ and orientation of cells, which has been introduced in section 2 and 3. In general, the absorbed energies decrease firstly and then reach to a plateau for the case of $d_1/l_0$ equals to 0.125. This observation means that the impact toughness is independent of $d_1/l_0$ as it is larger than 0.125. It can be found that the $d_1/l_0$ has an

obvious influence on absorbed energies in temperature range $20°C \sim -40°C$. However, the influence of the $d_1/l_0$ on absorbed energies turns to be increasingly minor when temperature lowers down to $-50°C$ and below.

### 4.1.2. The effect of residual stresses on impact toughness

To study the influence of the residual stresses on fracture in the transition region, a constant $d_1/l_0 = 0.125$ and varying $\Delta CTE$ are applied to generate residual stresses, e.g., Fig. 4(c). The absorbed energies at different temperature vs. $\Delta CTE$ are plotted in Fig. 6. It can be found that the residual stress has a significant influence on the absorbed energy in temperature range $20°C \sim -40°C$. However, the influence of the residual stress on absorbed energy continuously declines with the decrease of temperature. At very low temperature (the lower-shelf), e. g.,-80°C, the influence of the residual stress on absorbed energy becomes relative small. In general, absorbed energies linearly increase with the $\Delta CTE$ before the $\Delta CTE$ becomes $0°C^{-1}$, beyond which the absorbed energies enter a saturated zone. Although the compressive residual stresses are generated ahead of the notch root in the cases with positive $\Delta CTE$, the residual stress level is not high enough to make a difference on the fracture, which is the reason for the presence of the saturation region of absorbed energy.

### 4.1.3. The effect of residual stresses on DBT

To evaluate the influence of residual stresses on the transition behavior, three $\Delta CTEs$, e.g., $-0.065$, $-0.04$ and $-0.015°C^{-1}$, that have more obvious influence on absorbed energy (see Fig. 6) are investigated.
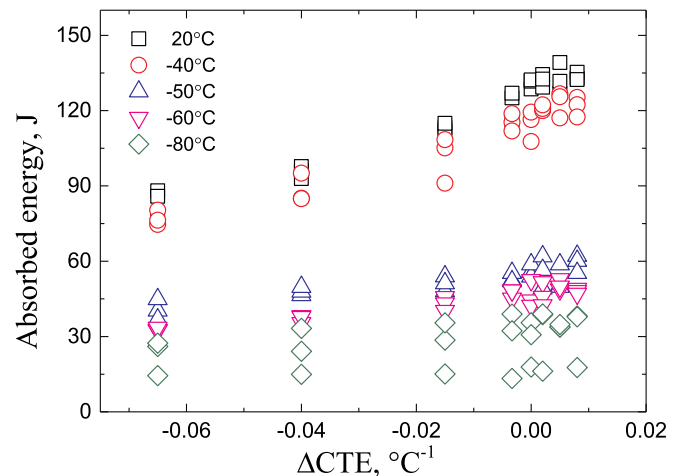


**Fig. 6.** The effect of the $\Delta CTE$ on the absorbed energy for the case with $d_1/l_0 = 0.125$.
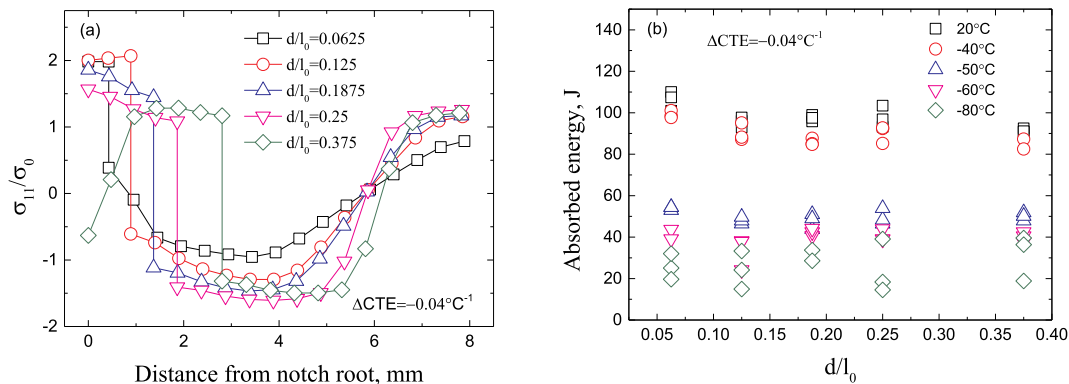


**Fig. 5.** The influence of the distance of interface apart from the notch root for the cases with a constant $\Delta CTE = $ -0.04$°C^{-1}$: (a) the distribution of opening stresses with different $d_1/l_0$, (b) the absorbed energies versus different $d/l_0$ at different temperature.

The absorbed energies vs. temperature in the full transition range are plotted in Fig. 7. It is observed that the transition curves generally shift to higher temperature with the increase of residual stresses. The upper-shelf energy (USE), e.g., the absorbed energies at temperature higher than −30 °C, dramatically decreases with the decrease of the ΔCTE, on which residual stresses exhibit a significant influence on DBT. Comparing with the influence on the upper-shelf of transition curve, residual stresses have a relatively weak effect on the absorbed energies in the transition region, −70 °C~−40 °C. Moreover, the influence of residual stresses on absorbed energies in this region continuously decays with the decrease of temperature. The absorbed energies in the lower shelf (LSE), −100 °C~−80 °C, basically do not change, which means that the residual stresses have almost no effect on the fracture. This indicates that the effect of residual stresses on DBT reduces with the decrease of temperature.

### 4.2. Configuration 2

In configuration 2, it is assumed that the whole damage zone is confined to the weld metal, see Figs. 2 and 3. Thus, only one constant distance of the interface to the notch root, e.g., $d_2/l_0 = 0.28125$, is considered. Like in configuration 1, residual stresses are generated by variable ΔCTE through changing $\alpha_2$ and fixing $\alpha_1$. The opening stress distribution of the case with a $\Delta CTE = -0.0033 °C^{-1}$ is presented in Fig. 8 (a). An interface formed by the inhomogeneity of CTE in two regions is presented in parallel to the crack plane. Inside the specimen, tensile stresses are produced in the center of specimen since the more pronounced contraction occurs by the higher CTE in this region, which agrees with the theory proposed by Simha et al. (2003). Since the interface is far from the notch root and parallel to the direction of crack plane, the stress in the vicinity of notch root is relatively low, which is different from that in configuration 1. The opening stresses $\sigma_{11}$ along the ligament in the middle of thickness (see Fig. 4(a)) normalized by $\sigma_0$ are presented in Fig. 8(b), in which different residual stresses are produced with ΔCTE. The normal components of residual stresses are also presented for the case with $\Delta CTE = -0.04 °C^{-1}$. The other normal stress components distribute with a similar feature to the opening stress. However, the opening stress $\sigma_{11}$ is lower than the other normal stresses, see Fig. 8(c).

#### 4.2.1. The effect of the residual stress on impact toughness
The residual stresses presented in Fig. 8(b) are applied to study their influence on fracture. The absorbed energies at different temperature vs.
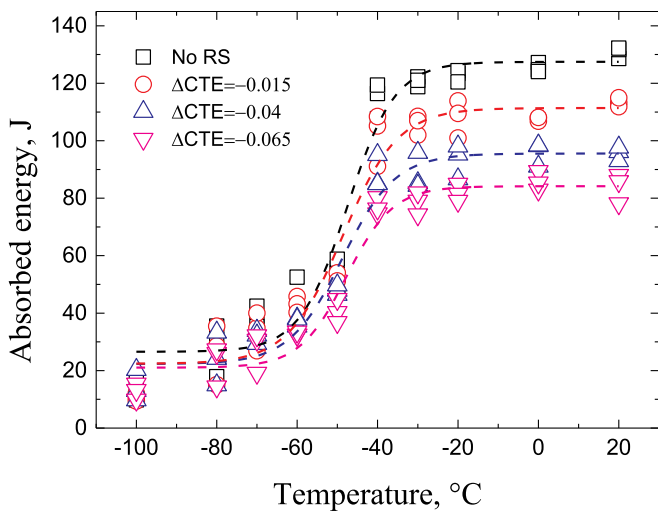


**Fig. 7.** The influence of residual stresses on the DBT. The distance of the interface apart from the notch root, $d_1/l_0 = 0.125$, and, $\alpha_1 = 0.01 °C^{-1}$. The data are fitted by the sigmoidal method.

ΔCTE are plotted in Fig. 9. It can be found that the ΔCTE has a significant influence on absorbed energy at higher temperature, e.g., 20 °C and −40 °C. However, the influence of the ΔCTE on absorbed energy continuously decreases with the decrease of temperature, e.g., −50 °C and −60 °C. At very low temperature (the lower-shelf), e.g., −80 °C, the influence of the ΔCTE on absorbed energy become insignificant. In general the absorbed energy has an approximate linear relationship with the difference of CET at the temperature above −80 °C before the ΔCTE reaches $0 °C^{-1}$. The absorbed energy is relatively stable when the ΔCTE is positive. This means the residual stress resulted by the positive ΔCTE is not high enough to affect the absorbed energy. The result presented in Fig. 9 is similar to the result shown in Fig. 6.

#### 4.2.2. The effect of residual stress on DBT
To study the influence of residual stresses on DBT, only three ΔCTEs, e.g., −0.065, −0.04 and −0.015 $°C^{-1}$, that have clear influence on absorbed energy (see Fig. 9), are investigated. The absorbed energies vs. temperature in the full transition range are plotted in Fig. 10. Comparing with the transition curve of the case without residual stress, the transition curves with different residual stresses generally shift to higher temperature with the increase of the residual stresses. The USE significantly decreases with the decrease of ΔCTE at temperatures higher than −30 °C. It appears that the residual stresses present a weaker effect on the absorbed energies at lower temperature. Comparing with the results presented in Fig. 7, it seems that the residual stress generated in the present configuration has a more pronounced effect on DBT than that produced in configuration 1 for the given residual stresses. It is hard to directly compare the influence of residual stress generated in both configurations on DBT because other aspects could also influence the results, for instance, the distance of interface to the notch root and the size of each region with variable CTE.

### 5. Discussions

Fracture occurs when the crack driving force, represented by a global parameter (*J* or *K*) as a function of applied load, exceeds its critical level. From this perspective, the influence of residual stress on the fracture can be effectively reflected by studying the change of crack driving force, *J* or *K*. According to the theory proposed by Simha et al., 2003, 2005, 2008, an additional crack driving force, e.g., $C_{inh}$, can be produced by the inhomogeneity of material. In section 4, the influence of residual stresses generated by the mismatch of CTE, e.g., ΔCTE, on DBT is investigated with two typical configurations of crack and interface. An additional driving force has been indeed found in both configurations through observing the distribution of residual stresses. However, the estimation of $C_{inh}$ in both configurations is a challenge for three-dimensional, real crack propagation, blunt notch and large scale yielding. Thus, the contribution of $C_{inh}$ to the fracture of material in the presence of residual stresses cannot be quantitatively evaluated in present work. It is known that the single fracture parameter, *J* or *K*, cannot solely describe the crack-tip stress and strain. The crack-tip stress triaxiality, namely constraint, exist in structures due to the geometry and loading mode. An alternative approach for the fracture prediction, e.g., micromechanical model, can accurately estimate the fracture propensity based on the examination of the crack-tip stress state. It has been reported that residual stresses can impact the constraint level at crack-tip (Liu et al., 2008; Ren et al., 2009), and in addition to that they can alter the crack driving force. To this end, the crack-tip constraint due to residual stress will be investigated so that the mechanism of residual stress effect on the fracture and DBT can be revealed.

O'Dowd and Shih (O'Dowd and Shih, 1991, 1992) have proposed a *J-Q* theory to describe the stress field near crack tip, which can be expressed by

$$\sigma_{ij} = \sigma_{ij}^{HRR} + Q\sigma_0 \left( \frac{r}{J/\sigma_0} \right)^q \tilde{\sigma}_{ij}(\theta, n) \tag{8}$$
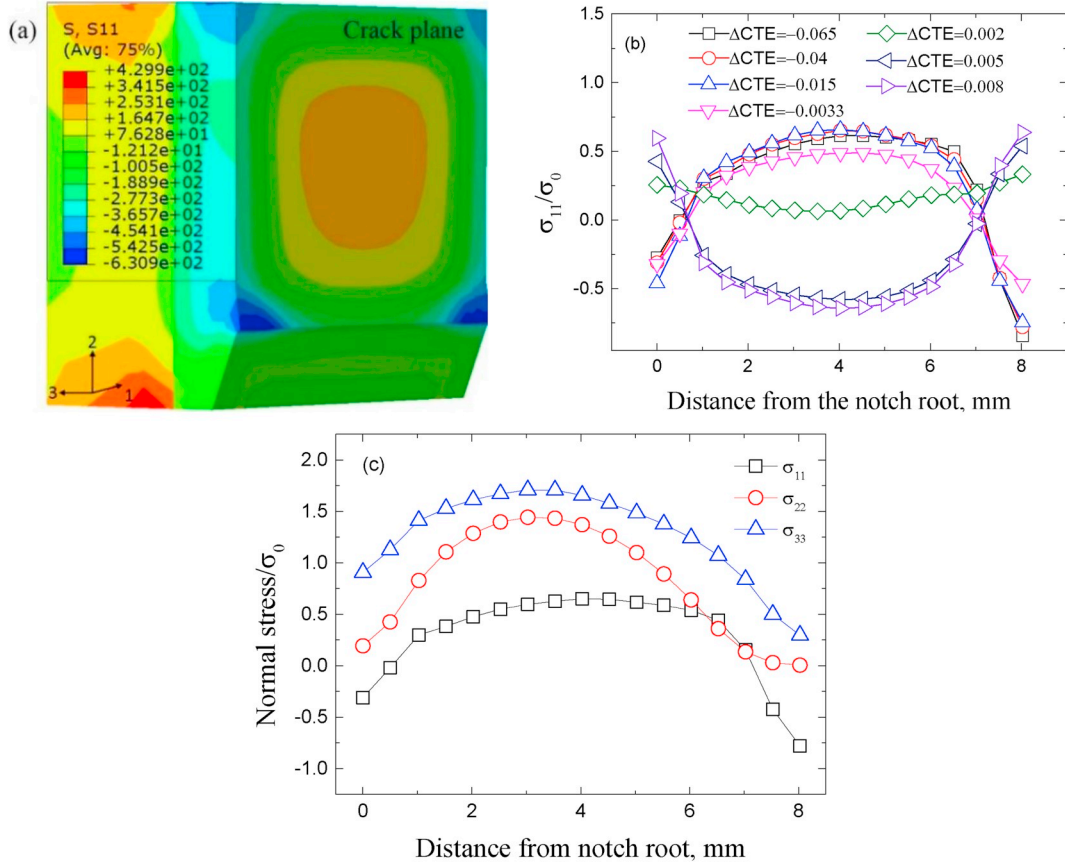
**Fig. 8.** Distribution of residual stress at the center of specimen along the ligament: (a) the pattern of opening stress, e.g., $\sigma_{11}$, for the case with the $\Delta CTE = -0.0033\,°C^{-1}$, (b) the opening stress of the cases with variable $\Delta CTE$, here $\alpha_1 = 0.01°C^{-1}$, (c) normal stresses of the case with the $\Delta CTE = -0.04\,°C^{-1}$.



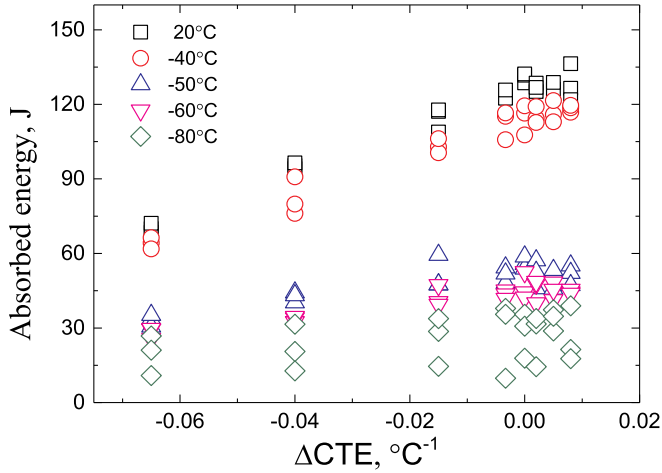**Fig. 9.** The effect of the $\Delta CTE$ on the absorbed energy.

where

$$\sigma_{ij}^{HRR} = \left(\frac{J}{\alpha_0 \varepsilon_0 \sigma_0 I_n r}\right)^{1/(n+1)} \sigma_0 \tilde{\sigma}_{ij}(\theta, n) \qquad (9)$$

$\sigma_{ij}^{HRR}$ is the J-controlled HRR stress field proposed by Huthinson (Hutchinson, 1968) and Rice and Rosengren (1968); $r$ and $\theta$ are polar coordinates centered at the crack tip; $n$ is the strain hardening exponent; $\varepsilon_0$ is the yield strain; $\alpha_0$ is a material constant; $\sigma_0$ is the yield stress; $I_n$ is an integration constant that depends on $n$; $q$ is a constant; $\tilde{\sigma}_{ij}$ is the
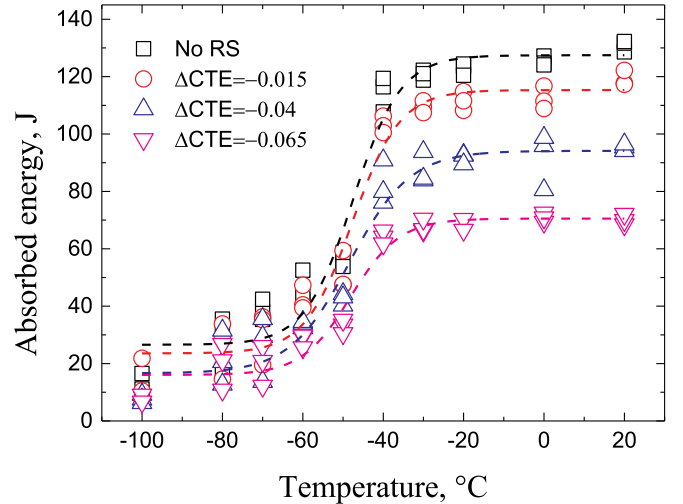


**Fig. 10.** The influence of residual stresses on the DBT. Data are fitted by the sigmoidal method.

dimensionless function of $\theta$ and $n$; Q is a hydrostatic stress parameter to quantify the crack-tip constraint caused by geometry or loading mode. Additional parameter, *M*, has been proposed by Zhang et al., 1996, 1997b to depict the constraint on the crack tip induced by the strength mismatch in the bi-material system of a weld component. The *J-Q-M* formulation has been developed to characterize the near-tip stress field in the presence of both geometry and material mismatch constraints (Zhang et al., 1997a), which also indicates that the constraint caused by

geometry and mismatch are independent of each other. Following the similar philosophy, Liu et al. (2008) and Ren et al. (2009) have proposed an approach to describe the near-tip stress field in presence of residual stress, which can be expressed by

$$\sigma_{ij}^{RS} = \sigma_{ij}^{NoRS} + \sigma_0 R(r, \theta, n, J, \sigma_0 \ldots)\delta_{ij} \tag{10}$$

where $\sigma_{ij}^{NoRS}$ is the near-tip stress field without residual stress, which can be described by Eqs. (8) and (9); $R$ is the constraint induced by residual stress, which is relevant to $r$, $\theta$, $n$, $J$ and $\sigma_0$ etc. The $R_{ij}$ can be estimated by

$$R_{ij} = \frac{\sigma_{ij}^{RS} - \sigma_{ij}^{NoRS}}{\sigma_0} \tag{11}$$

The notch-tip constraints induced by the residual stresses are calculated in terms of Eq. (11) at the same loading time. The constraint near notch root in the area of interest (see Fig. 4(a)) caused by residual stress vs. the loading time in both configurations of Charpy specimen tested at room temperature are plotted in Fig. 11. It can be observed that in general a positive constraint can be introduced into the specimen near the notch tip when a negative $\Delta CTE$ is adopted in both configurations, see Fig. 11(a) ~ (b). On the contrary, a negative constraint is produced in the vicinity of notch tip when a positive $\Delta CTE$ is used, see Fig. 11 (c) ~ (d). It also can be found that the constraints near the notch tip induced by the residual stresses generated by either negative or positive $\Delta CTE$ gradually decays as external load increases. This phenomenon has also been reported by Liu et al. (2008) and Ren et al. (2009). Recall the residual stress distributions in two configurations, since the interface formed by the mismatch of CTE is perpendicular to the crack propagation in configuration 1, residual stresses concentrated on the area near the notch root, see Fig. 4(b). However, residual stresses in configuration 2 are mainly distributed in the center of crack plane away from the notch root, see Fig. 8(b), because the interface is parallel to the crack

extension. It is found that the initial constraints near notch tip induced by the residual stresses in configuration 1 is generally higher than those in configuration 2, see Fig. 11 (a) ~ (d). It is also noticed that the constraints near notch root induced by the residual stresses in configuration 1 vanish nearly at 0.12 ms (see Fig. 11(a) and (c)) which is much earlier than those in configuration 2, e.g., around 0.24 ms (see Fig. 11(b) and (d)). This implies that the residual stresses generated by $\Delta CTE$ in configuration 1 changes more easily by the external loading than those in configuration 2. In addition, it is observed that opening mode constraint, e.g., $R_{11}$, in configuration 1 is one of the dominant components of the stress triaxiality near the notch tip caused by residual stress. In configuration 2, the constraint along thickness direction, e.g., $R_{33}$, is the dominant component. This means that opening mode residual stress is not the sole factor which influences the fracture as one might think intuitively, which also indicates the necessity of the analysis on the triaxial stress state at crack-tip caused by the residual stress for studying fracture with residual stress presented.

To reveal the effect of constraint induced by the residual stress on fracture, the element in the middle of notch root, so-called the reference element, is analyzed since this element tends to fail first due to the high constraint in the middle of thickness. Opening stresses of the reference element normalized by the yield stress at room temperature vs. loading time are plotted in Fig. 12 for the Charpy specimen tested at $20\,^{\circ}C$ and $-80\,^{\circ}C$. It is found that in both configurations at two different temperatures the reference element in the specimen with residual stress generated by $\Delta CTE = -0.015\,^{\circ}C^{-1}$ failed relatively earlier than that in the specimen without residual stress. On the contrary, the reference element in the specimen with residual stress generated by $\Delta CTE = 0.008\,^{\circ}C^{-1}$ in both configurations failed comparatively later than that in the specimen without residual stress at both temperatures. If the curves presented in Fig. 12 can be deemed as the degradation locus of material under ductile damage, they are generally close to each other besides that
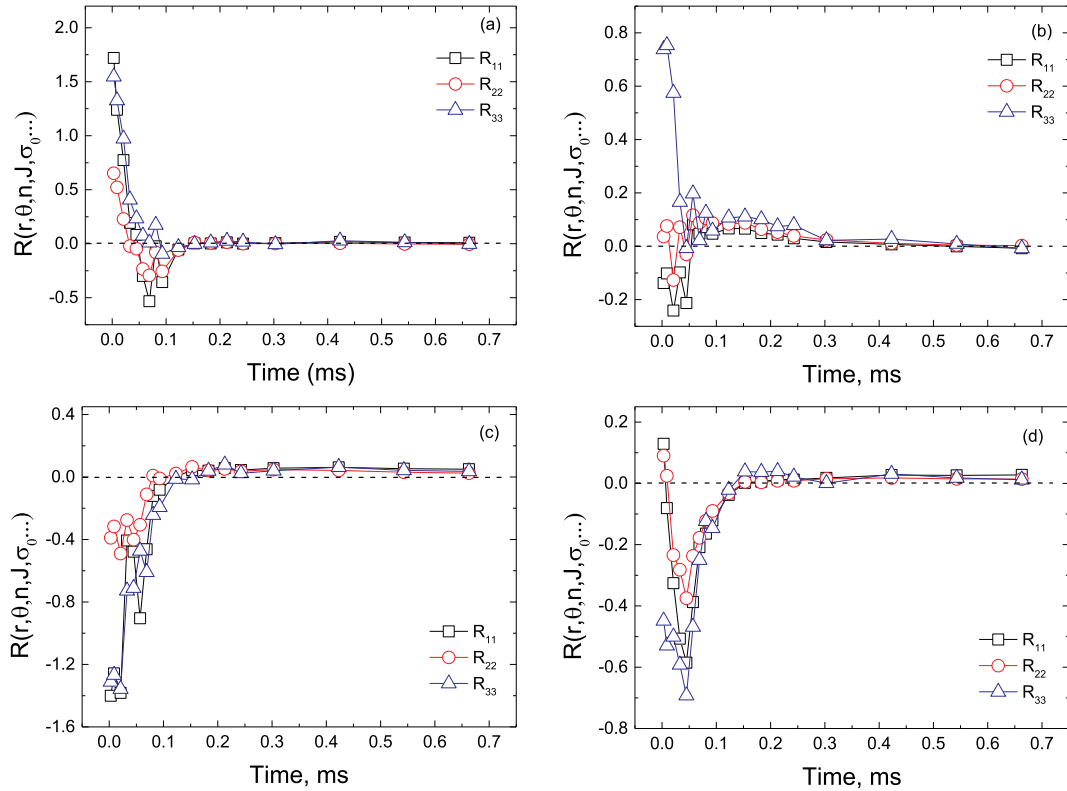


**Fig. 11.** The evaluation of notch-tip constraint induced by residual stresses at the position away from the notch root with a distance of $\delta/l_0 = 0.0625$ for cases at room temperature: (a) $\Delta CTE = -0.015\,^{\circ}C^{-1}$ in configuration 1, (b) $\Delta CTE = -0.015\,^{\circ}C^{-1}$ in configuration 2, (c) $\Delta CTE = 0.008\,^{\circ}C^{-1}$ in configuration 1, (d) $\Delta CTE = 0.008\,^{\circ}C^{-1}$ in configuration 2.

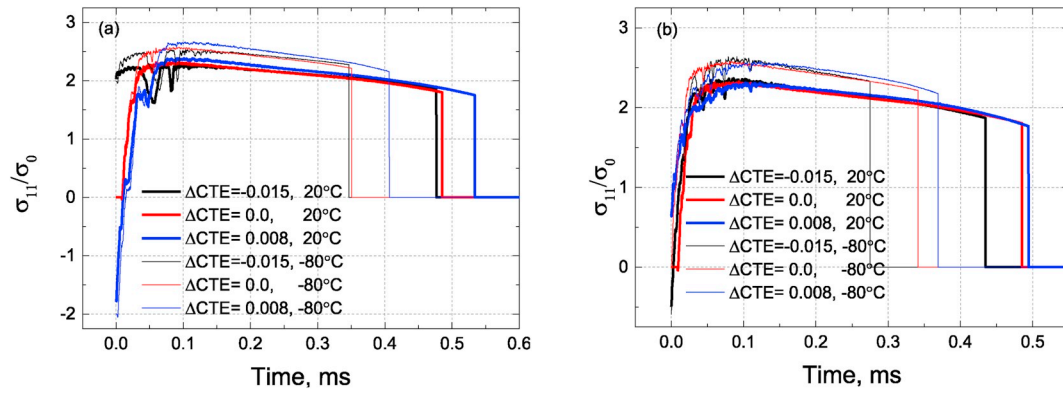**Fig. 12.** The opening stresses of the reference element of Charpy specimen tested at $20\,°C$ and $-80\,°C$: (a) configuration 1, (b) configuration 2.

they are in the very beginning loading stage due to the different constraint caused by residual stress. Consequently, the earlier occurrence of failure in the reference element corresponds to a higher opening stresses at the moment of failure. With the increase of $\Delta CTE$ in both configurations (e.g., the positive constraint transforming to a negative one), the period for the degradation of material in the reference element becomes longer. This means that the lower impact toughness of material or structure could be aroused by the more positive constraint in the vicinity of near notch tip by high residual stress. To prove this, opening stresses of the reference elements at the moment of failure vs. $\Delta CTE$ is plotted for the case at room temperature in Fig. 13(a) and Fig. 14(a) for all cases with variable residual stress in both configurations. It is found that opening stresses in reference elements when failure occurs linearly decrease with the increase of $\Delta CTE$. When the failure occurs in reference elements, the force and absorbed energies of Charpy specimen vs. $\Delta CTE$ are plotted in Figs. 13(b) and 14(b) for both configurations. It is found that the force and absorbed energy increase linearly with the increase of the $\Delta CTE$. It can be also observed that the variation of both force and absorbed energy with $\Delta CTE$ shown in Figs. 13(b) and 14(b) are consistent with that of total absorbed energy when specimen completely breaks at room temperature, see Figs. 6 and 9. The results similar with those presented in Figs. 13 and 14 are also obtained for the cases with different $\Delta CTE$ at $-80\,°C$. Then, it can be concluded that the reduction of absorbed energy of specimens with the decrease of $\Delta CTE$ is ascribed for the increase of constraint in the vicinity of notch root induced by the residual stresses in both configurations (see Figs. 6 and 9). Similar results related to the effect of residual stress on the fracture has been reported by Ren et al. (Ren et al., 2009, 2010, 2011).

The role of the constraint near the notch root resulted by the residual stress normally works for both ductile and brittle fracture, see Fig. 12. However, it is observed that with the decrease of $\Delta CTE$ the reduction of absorbed energy at high temperature is more pronounced than that at low temperature, see Figs. 6 and 9. It can be found in Figs. 7 and 10 that

the drop of absorbed energy with the decrease of $\Delta CTE$ gradually decays as temperature decreases, and that the residual stress presents a significant influence on the DBT at higher temperature, from which the upper-shelf of the transition curve changes dramatically. This means that the effect of constraint induced by residual stress on DBT exhibits a temperature dependent feature. To explain this, constraints near the notch root in the area of interest (see Fig. 4(a)) induced by residual stresses of cases with $\Delta CTE = $ -0.015 $°C^{-1}$ at different temperature in both configurations vs. the displacement of striker are plotted in Fig. 15. It is found from Fig. 15 (a) ~ (c) that in configuration 1 constraints induced by residual stress at all temperatures decay with the displacement of striker in the same manner until they totally vanish. However, the initial constraint near notch tip induced by residual stress at higher temperature is generally higher than that at lower temperature, e.g., $R_{11}$, $R_{22}$. The same results in the configuration 2 can be also observed from Fig. 15 (d) ~ (f). However, the significant difference among the initial constraints near notch tip in configuration 2 occurs on the $R_{22}$ and $R_{33}$. Recall Eq. (11), when the same residual stress is generated in the specimen, the constraint near the notch tip depends on the yield stress and strain hardening. For the material studied, the yield stress increases with the decrease of temperature, and the strain hardening is not obviously changed see Fig. 5(a) in the ref. (Li et al., 2019). Therefore, the initial constraint at notch tip induced by the residual stress decreases with the temperature mainly connects with the variation of yield stress of material at different temperature.

Charpy impact tests at different temperature are modelled after residual stresses introduced into the specimens. According to Eq. (10), residual stress generated following the method introduced in section 3.1 is relevant to the flow property of material, e.g., yield stress and strain hardening. However, due to the limitation of present method, it is unlikely to define two different flow properties of material for two independent simulation steps, e.g., in a case using flow property of material at $20\,°C$ for the residual stress generation in step 1, while adopting flow
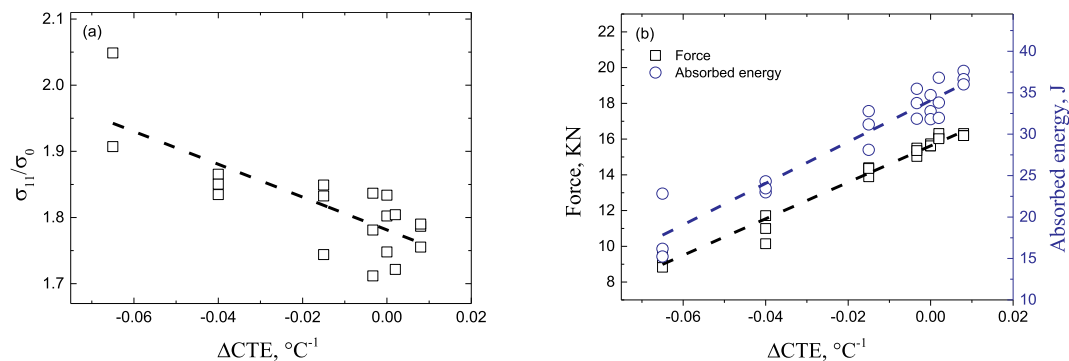


**Fig. 13.** Failure of the reference element of the Charpy tests at $20\,°C$ in configuration 1: (a) opening stress, (b) force and absorbed energy.
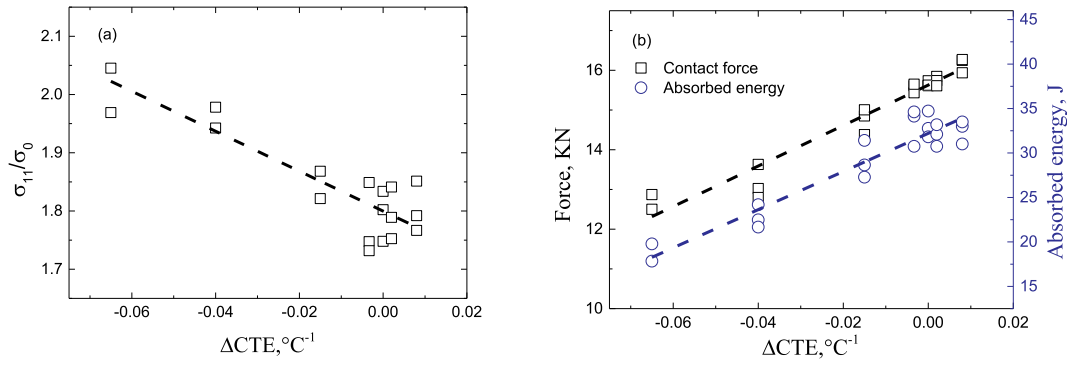
**Fig. 14.** Failure of the reference element of the Charpy tests at 20 °C in configuration 2: (a) opening stress, (b) force and absorbed energy.
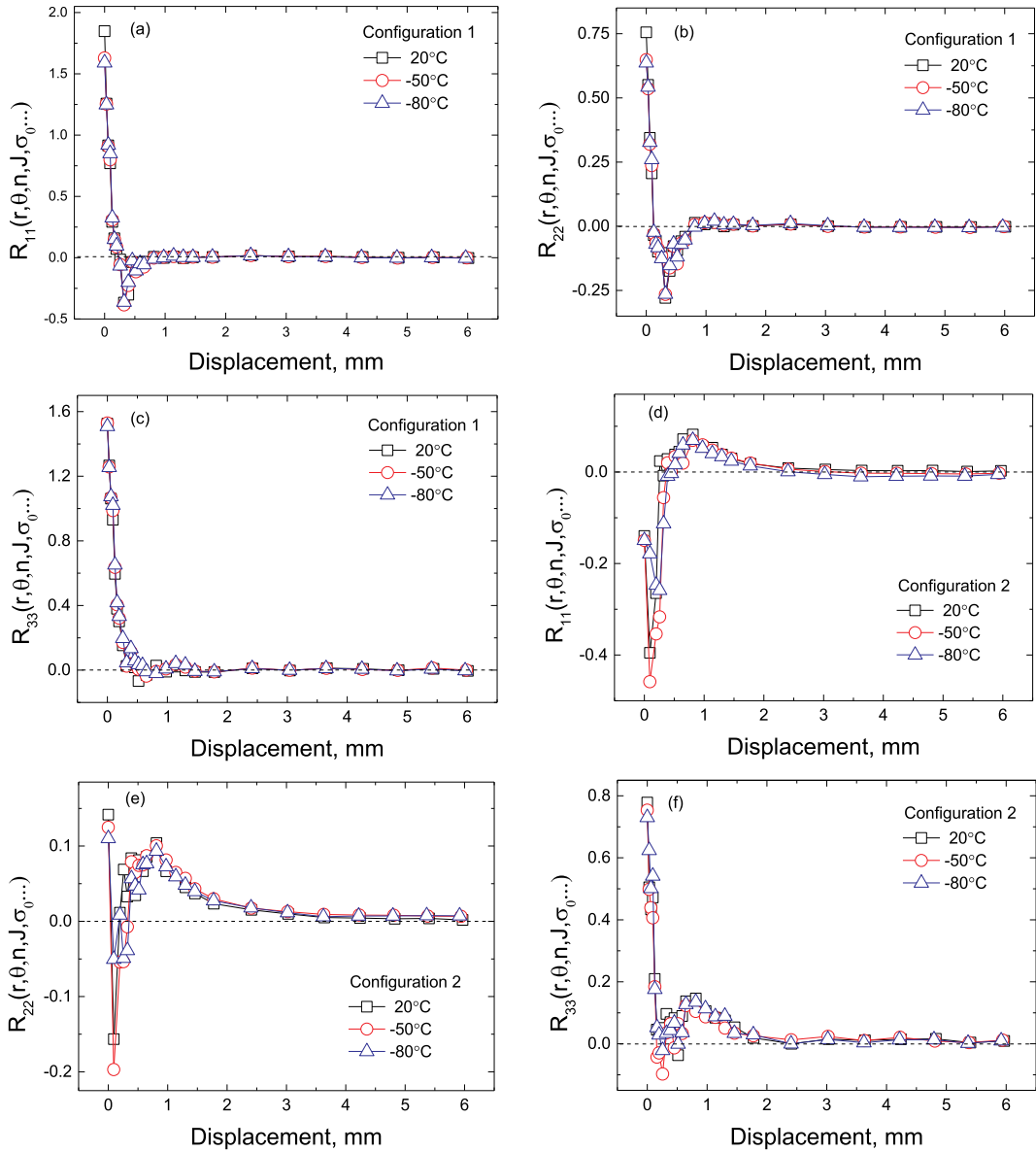


**Fig. 15.** The notch-tip constraints induced by residual stresses at the position away from the notch root with a distance of $\delta/l_0 = 0.0625$ in both configurations of cases with $\Delta CTE = -0.015\,°C^{-1}$ at different temperature: (a) ~ (c) $R_{11}$, $R_{22}$ and $R_{33}$ in configuration 1; (d) ~ (f) $R_{11}$, $R_{22}$ and $R_{33}$ in configuration 2.

property at $-20\,°C$ for the Charpy impact test simulation in step 2. The individual flow property of material at test temperature is simultaneously utilized for both independent steps, which could produce higher

initial residual stresses in the specimens for Charpy impact test at lower temperatures. For instance, when the lowest $\Delta CTE = -0.065\,°C^{-1}$, is adopted in both configurations, the residual stress in specimen for

Charpy impact test at $-100\,°C$ is about 10% higher than that for test at room temperature. Therefore, it can be inferred that the more obvious declining trend of the influence of residual stress on DBT can be expected than that found in Figs. 7 and 10, if residual stresses generated in specimens could keep at the same level at different temperature.

In the present work, two configurations of the crack and interface formed by the mismatch of CTE in a bi-material specimen have been designed to generate residual stress and study the effect of residual stress on fracture. The influence of residual stress on the DBT has been studied by using CAFE method implemented with a temperature dependent effective surface energy proposed by the authors (Li et al., 2019). A significant influence of residual stress on the fracture and DBT has been found, and the mechanism for the role of residual stress on DBT has been discussed. However, there are still some limitations existing in the present work. Firstly, the eigenstrain method has been employed to introduce the residual stress in which a unit temperature decrease is applied with the artificial CTE (see Eq. (7)) rather than using coupled thermo-mechanics and metallurgical analysis. In practice, residual stresses in the weldment are normally produced during cooling process, e.g., liquid state of the material at high temperature to solid state at room temperature. When specimen is cooled down to the test temperature, the residual stresses could increase more or less depending on the specific test temperature. Therefore, the change of residual stress in the specimen during the cooling process, e.g., from room temperature to the test temperature, is unlikely captured in the present study. Secondly, the release of residual stress in the process of the V-notch introduced into the test specimen has not been taken into account. This is another limitation of present work. Finally, the residual stress generated in the specimen changes with different temperature due to the limitation of present method, which has been introduced in detail in above.

## 6. Conclusions

In the present study, the CAFE method, a micro-mechanical approach, which can capture the competition of ductile fracture and cleavage, has been successfully applied to study the influence of residual stress on DBT. Inspired by the studies on the effect of material inhomogeneity by Simha et al., 2003, 2005, 2008 and the work by Rakin et al. (2009), two configurations of crack and interface formed by the mismatch of CTE in a bi-material specimen, e.g., the interface perpendicular and parallel to the crack propagation, have been designed to introduce residual stress and study the effect of residual stress on fracture. Different residual stresses have been generated by controlling the mismatch of CTE, e.g., $\Delta CTE$, in both configurations. With the residual stresses initially generated in the Charpy specimen, their influence on DBT of a bi-material specimen has been studied by utilizing the CAFE method implemented with a temperature dependent surface energy proposed by the authors (Li et al., 2019). To reveal the mechanism of residual stress on DBT, constraints in the vicinity of notch root induced by residual stresses have been estimated in both configurations.

Although the distribution of generated residual stresses present different features in the two configurations, it is observed that tensile residual stress is generated in the region where a higher CTE is employed in both configurations, and vice versa. The results accord with the findings in the Ref. (Rakin et al., 2009). It is found that the initial constraint caused by the residual stress in configuration 1 is higher than that in configuration 2 when the same $\Delta CTE$ is adopted. However, with the increase of external load, the constraint induced by residual stress in configuration 1 decays much quicker than that in configuration 2.

It is observed that in both configurations the absorbed energy of specimen decreases with the increase of residual stress (e.g., corresponding to the decrease of $\Delta CTE$). As a consequence, the DBT curves of two configurations generally shift to higher temperature. The reason for the influence of residual stress on the impact toughness (e.g., absorbed energy) is that the constraint induced by the residual stresses on notch root facilitates fracture.

A significant change on DBT due to the residual stress in both configurations can be observed at high temperature, e.g., the upper-shelf of transition curves. However, the influence of residual stresses on the absorbed energies in both configurations shows a declining trend with the decrease of temperature.

## References

ASTM E23-18, 2018. Standard Test Methods for Notched Bar Impact Testing of Metallic Materials.

Aloraier, A., Al-Mazrouee, A., Price, J.W.H., Shehata, T., 2010. Weld repair practices without post weld heat treatment for ferritic alloys and their consequences on residual stresses: a review. Int. J. Press. Vessel. Pip. 87, 127–133.

Chen, C.R., Pascual, J., Fischer, F.D., Kolednik, O., Danzer, R., 2007. Prediction of the fracture toughness of a ceramic multilayer composite – modeling and experiments. Acta Mater. 55, 409–421.

Coules, H.E., Horne, G.C.M., Abburi Venkata, K., Pirling, T., 2018. The effects of residual stress on elastic-plastic fracture propagation and stability. Mater. Des. 143, 131–140.

Faes, K., Dhooge, A., De Baets, P., Afschrift, P., 2009. New friction welding process for pipeline girth welds—welding time optimisation. Int. J. Adv. Manuf. Technol. 43, 982–992.

Fischer, F.D., Predan, J., Kolednik, O., Simha, N.K., 2007. Application of material forces to fracture of inhomogeneous materials: illustrative examples. Arch. Appl. Mech. 77, 95–112.

Hill, M., Panontin, T., 1999. Effect of Residual Stress on Brittle Fracture Testing, Effect of Residual Stress on Brittle Fracture Testing.

Hutchinson, J.W., 1968. Singular behaviour at the end of a tensile crack in a hardening material. J. Mech. Phys. Solids 16, 13–31.

Jun, T.-S., Korsunsky, A.M., 2010. Evaluation of residual stresses and strains using the Eigenstrain reconstruction method. Int. J. Solids Struct. 47, 1678–1686.

Kolednik, O., Predan, J., Fischer, F.D., 2010. Cracks in inhomogeneous materials: comprehensive assessment using the configurational forces concept. Eng. Fract. Mech. 77, 2698–2711.

Kolednik, O., Predan, J., Shan, G.X., Simha, N.K., Fischer, F.D., 2005. On the fracture behavior of inhomogeneous materials—A case study for elastically inhomogeneous bimaterials. Int. J. Solids Struct. 42, 605–620.

Lei, Y., O'Dowd, N.P., Webster, G.A., 2000. Fracture mechanics analysis of a crack in a residual stress field. Int. J. Fract. 106, 195–216.

Li, Y., Ren, X., He, J., Zhang, Z., 2018. Constraint effect on the brittle-to-ductile transition of single-crystal iron induced by dislocation mobility. Int. J. Mech. Sci. 149, 212–223.

Li, Y., Shterenlikht, A., Ren, X., He, J., Zhang, Z., 2019. CAFE based multi-scale modelling of ductile-to-brittle transition of steel with a temperature dependent effective surface energy. Mater. Sci. Eng., A 755, 220–230.

Liu, J., Zhang, Z.L., Nyhus, B., 2008. Residual stress induced crack tip constraint. Eng. Fract. Mech. 75, 4151–4166.

Mahmoudi, A.H., Truman, C.E., Smith, D.J., 2008. Using local out-of-plane compression (LOPC) to study the effects of residual stress on apparent fracture toughness. Eng. Fract. Mech. 75, 1516–1534.

Meith, W.A., Hill, M.R., 2002. Domain-independent values of the J-integral for cracks in three-dimensional residual stress bearing bodies. Eng. Fract. Mech. 69, 1301–1314.

Mirzaee-Sisan, A., Truman, C.E., Smith, D.J., Smith, M.C., 2007. Interaction of residual stress with mechanical loading in a ferritic steel. Eng. Fract. Mech. 74, 2864–2880.

Mirzaee-Sisan, A., Truman, C.E., Smith, D.J., Smith, M.C., 2008. Interaction of residual stress with mechanical loading in an austenitic stainless steel. Fatigue Fract. Eng. Mater. Struct. 31, 223–233.

Moshayedi, H., Sattari-Far, I., 2015. The effect of welding residual stresses on brittle fracture in an internal surface cracked pipe. Int. J. Press. Vessel. Pip. 126–127, 29–36.

Mura, T., 1987. Micromechanics of Defects in Solids. Springer Scince & Business Media.

Niwa, M., Shikama, T., Yonezu, A., 2015. Mechanism of hydrogen embrittlement cracking produced by residual stress from indentation impression. Mater. Sci. Eng., A 624, 52–61.

Nose, M., Amano, H., Okada, H., Yusa, Y., Maekawa, A., Kamaya, M., Kawai, H., 2017. Computational crack propagation analysis with consideration of weld residual stresses. Eng. Fract. Mech. 182, 708–731.

O'Dowd, N.P., Shih, C.F., 1991. Family of crack-tip fields characterized by a triaxiality parameter—I. Structure of fields. J. Mech. Phys. Solids 39, 989–1015.

O'Dowd, N.P., Shih, C.F., 1992. Family of crack-tip fields characterized by a triaxiality parameter—II. Fracture applications. J. Mech. Phys. Solids 40, 939–963.

Panontin, T.L., Hill, M.R., 1996. The effect of residual stresses on brittle and ductile fracture initiation predicted by micromechanical models. Int. J. Fract. 82, 317–333.

Rakin, M., Kolednik, O., Medjo, B., Simha, N.K., Fischer, F.D., 2009. A case study on the effect of thermal residual stresses on the crack-driving force in linear-elastic bimaterials. Int. J. Mech. Sci. 51, 531–540.

Ren, X.B., Zhang, Z.L., Nyhus, B., 2009. Effect of residual stresses on the crack-tip constraint in a modified boundary layer model. Int. J. Solids Struct. 46, 2629–2641.

Ren, X.B., Zhang, Z.L., Nyhus, B., 2010. Effect of residual stresses on ductile crack growth resistance. Eng. Fract. Mech. 77, 1325–1337.

Ren, X.B., Zhang, Z.L., Nyhus, B., 2011. Effect of residual stress on cleavage fracture toughness by using cohesive zone model. Fatigue Fract. Eng. Mater. Struct. 34, 592–603.

Rice, J.R., Rosengren, G.F., 1968. Plane strain deformation near a crack tip in a power-law hardening material. J. Mech. Phys. Solids 16, 1–12.

Rousselier, G., 1987. Ductile fracture models and their potential in local approach of fracture. Nucl. Eng. Des. 105, 97–111.

Shterenlikht, A., 2003. 3D CAFE Modelling of Transitional Ductile-Brittle Fracture in Steel. The University of Sheffield, UK.

Shterenlikht, A., Howard, I.C., 2004. Cellular Automata Finite Element (CAFE) modelling of transitional ductile-brittle fracture in steel. In: The 15th European Conference of Fracture (ECF15). KTH, Stockholm, Sweden.

Shterenlikht, A., Howard, I.C., 2006. The CAFE model of fracture—application to a TMCR steel. Fatigue Fract. Eng. Mater. Struct. 29, 770–787.

Shterenlikht, A., Margetts, L., 2015. Three-dimensional cellular automata modelling of cleavage propagation across crystal boundaries in polycrystalline microstructures.

In: Proceedings of the Royal Society of London A: Mathematical, Physical and Engineering Sciences, vol. 471.

Simha, N.K., Fischer, F.D., Kolednik, O., Chen, C.R., 2003. Inhomogeneity effects on the crack driving force in elastic and elastic–plastic materials. J. Mech. Phys. Solids 51, 209–240.

Simha, N.K., Fischer, F.D., Kolednik, O., Predan, J., Shan, G.X., 2005. Crack tip shielding or anti-shielding due to smooth and discontinuous material inhomogeneities. Int. J. Fract. 135, 73–93.

Simha, N.K., Fischer, F.D., Shan, G.X., Chen, C.R., Kolednik, O., 2008. J-integral and crack driving force in elastic–plastic materials. J. Mech. Phys. Solids 56, 2876–2895.

Stec, M., Faleskog, J., 2009. Micromechanical modeling of grain boundary resistance to cleavage crack propagation in ferritic steels. Int. J. Fract. 160, 151.

Toribio, J., Kharin, V., Lorenzo, M., Vergara, D., 2011. Role of drawing-induced residual stresses and strains in the hydrogen embrittlement susceptibility of prestressing steels. Corros. Sci. 53, 3346–3355.

Withers, P.J., 2007. Residual stress and its role in failure. Rep. Prog. Phys. 70, 2211.

Zamani, E., Liaghat, G.H., 2012. Explosive welding of stainless steel–carbon steel coaxial pipes. J. Mater. Sci. 47, 685–695.

Zhang, Z., Hauge, M., Thaulow, C., 1997a. The Effect of T -stress on the Near Tip Stress Field of an Elastic-Plastic Interface Crack.

Zhang, Z.L., Hauge, M., Thaulow, C., 1996. Two-parameter characterization of the near-tip stress fields for a bi-material elastic-plastic interface crack. Int. J. Fract. 79, 65–83.

Zhang, Z.L., Thaulow, C., Hauge, M., 1997b. Effects of crack size and weld metal mismatch on the has cleavage toughness of wide plates. Eng. Fract. Mech. 57, 653–664.